



## Article

# Potential of the Biomass Waste Originating from *Saccharum officinarum* as a Fenton Precursor for the Efficient Oxidation of Azo Dye from an Aqueous Stream

Ehssan Ahmed Hassan <sup>1,2,\*</sup>, Maha A. Tony <sup>3,4,\*</sup>, Hossam A. Nabwey <sup>3,5,\*</sup>  and Mohamed M. Awad <sup>5,6,\*</sup> 

<sup>1</sup> Department of Biology, College of Science and Humanities, Prince Sattam bin Abdulaziz University, Alkharj 11942, Saudi Arabia

<sup>2</sup> Department of Zoology, Faculty of Science, Suez Canal University, Ismailia 41522, Egypt

<sup>3</sup> Basic Engineering Science Department, Faculty of Engineering, Menoufia University, Shebin El-Kom 32511, Egypt

<sup>4</sup> Advanced Materials/Solar Energy and Environmental Sustainability (AMSEES) Laboratory, Faculty of Engineering, Menoufia University, Shebin El-Kom 32511, Egypt

<sup>5</sup> Department of Mathematics, College of Science and Humanities in Al-Kharj, Prince Sattam bin Abdulaziz University, Al-Kharj 11942, Saudi Arabia

<sup>6</sup> Department of Mathematics, Faculty of Science, Suez Canal University, El-Sheik Zayed, Ismailia 41522, Egypt

\* Correspondence: e.basiouny@psau.edu.sa (E.A.H.); dr.maha.tony@gmail.com (M.A.T.); eng\_hossam21@yahoo.com (H.A.N.); m.abdelgalil@psau.edu.sa (M.M.A.)

**Abstract:** In the current investigation, elements extracted from *Saccharum officinarum* were identified as exporters of Fenton catalysts. *Saccharum officinarum* was soaked in an alkali prior to acidic treatment and then subjected to pyrolysis for elemental recovery. X-ray diffraction (XRD) and scanning electron microscopy (SEM) augmented with energy-dispersive X-ray spectroscopy (EDX) were used to identify the prepared catalyst. The material was combined with hydrogen peroxide, which led to Fenton's reaction. Then, the modified Fenton system was applied to eliminate the textile dye, named Bismarck Brown Azo dye, contaminating the aqueous effluent. Response surface methodological model (RSM) analysis was used to identify the most effective operational parameters, and the model set the optimized values as 39 and 401 mg/L for *Saccharum officinarum* and H<sub>2</sub>O<sub>2</sub> doses, respectively, at pH 2.9. The maximum Bismarck Brown Azo dye removal achieved was 85%. Increasing the temperature to 60 °C improved the dye oxidation efficiency. However, the dye treatment efficacy was reduced when the dye loading increased. Additionally, the kinetic rate order was investigated and the system was fitted to second-order rate reaction kinetics. The thermodynamic variables show that the reaction is endothermic and non-spontaneous.

**Keywords:** Bismarck Brown dye; oxidation; waste management; kinetics; thermodynamics



**Citation:** Hassan, E.A.; Tony, M.A.; Nabwey, H.A.; Awad, M.M. Potential of the Biomass Waste Originating from *Saccharum officinarum* as a Fenton Precursor for the Efficient Oxidation of Azo Dye from an Aqueous Stream. *Processes* **2023**, *11*, 1394. <https://doi.org/10.3390/pr11051394>

Academic Editor: Slawomir Stelmach

Received: 3 April 2023

Revised: 24 April 2023

Accepted: 25 April 2023

Published: 4 May 2023



**Copyright:** © 2023 by the authors. Licensee MDPI, Basel, Switzerland. This article is an open access article distributed under the terms and conditions of the Creative Commons Attribution (CC BY) license (<https://creativecommons.org/licenses/by/4.0/>).

## 1. Introduction

Agro-industrial waste residuals produced indiscriminately constitute extreme environmental pollution. However, currently, such waste is attracting researchers' attention since it can be converted into wealth [1,2]. For instance, Gu et al. [3] valorized sewage sludge to be used as a catalyst for wastewater elimination. Ullah et al. [4] applied sugarcane bagasse to adsorb dye from an aqueous stream. Sugarcane bagasse, or *Saccharum officinarum*, is an agro-industrial waste by-product, and its lignocellulosic residuals have attracted scientists' attention for their use as adsorbent materials [5]. Several authors have applied chemical enhancement to improve the activity of such materials [6,7]. Sun et al. [8] enhanced *Saccharum officinarum* by etherification with extra stearic acid. Ahamad et al. [9] washed *Saccharum officinarum* with NaOH and then sonicated it to improve its catalytic activity. Xiong et al. [10] used various acids to treat such waste material. However, the use of *Saccharum officinarum* as an adsorbent material is not considered an ideal solution since it

only transfers the pollutants' phase, with no respect for their mineralization [11]. However, due to the chemical nature of modified *Saccharum officinarum*, which possesses several elements, as well as its reasonably high surface area [12], it can be used as a photocatalyst.

The primary goal of academics and scientists is to identify an industrial ecology approach that will lead to harmless end products, the aim being to diminish persistent toxic materials [13]. In this regard, Fenton's reagent is proposed as an environmentally sustainable benign reagent [14,15]. Fenton's reaction is one of the most advanced oxidation processes (AOPs) and is categorized as a rapid and efficient process. Fenton's reaction is based on the oxidization of iron metal with hydrogen peroxide to initiate the additional charge production of highly reactive species called hydroxyl radicals, which are mineralizing pollutants. However, the cost of chemical precursors and the acidic working pH range prevent the use of Fenton's treatment in real applications [16]. Thus, it is important to identify an alternative iron source instead of fresh chemicals for use as a photocatalyst. The combination of metals, i.e., aluminum and manganese, with iron from a waste source to serve as a source of the Fenton heterojunction is a good alternative [17,18]. Additionally, an augmented copper–carbon composite can be introduced as the source of a heterogeneous Fenton-like system. Such elements, when augmented with hydrogen peroxide, produce non-specific hydroxyl radicals, which are the horsepower of oxidizing reactions since such radicals attack the wide range of pollutants in aqueous streams. Thus, this system has a high chance of avoiding Fenton restrictions because it can solve the associated system problems [19,20].

Since the 20th century, there is growing awareness about the large amounts of pollutants produced by industrial activities and their effect on the environment. Water shortages are causing severe damage and must be addressed to meet ecological societal needs [21,22]. Enormous amounts of toxic effluents from the textile industry are discharged into canals and drains, causing severe destruction of the environmental ecosystem. The textile industry is among the industrial sectors that require substantial quantities of water in the various processing steps [23]. Aqueous effluents from the industry contain fibers, metals, suspended solids, and solvents and have high biological oxygen demand (BOD) and chemical oxygen demand (COD). Due to restrictive environmental regulations worldwide and public health safety rules, it is important for such effluents to be remediated prior to their discharge [24,25].

To the best of the authors' knowledge, the research on the modulation of *Saccharum officinarum* as a photocatalytic material to be an exporter of Fenton's reagent is deficient. The current study is focused on using bagasse residuals, which are the waste material left behind when *Saccharum officinarum* is processed, as a source of elements to be used as a photocatalyst for textile dye elimination. The residuals were treated and calcined catalyst analysis and characterization were performed to investigate their activity. The impact of the operational variables, i.e., the *Saccharum officinarum* catalyst and the dose of the hydrogen peroxide reagents, the impact of the pH level in the aqueous solution, dye loading, and wastewater temperature, on the oxidation reaction were evaluated. Response surface methodology was applied for statistical analysis and optimization of the operational parameters.

## 2. Materials and Methods

### 2.1. Aqueous Dye Effluent

Commercial textile dye named Bismarck Brown dye (supplied by Macsen Lab. Udaipur, Rajasthan, 313024, India), with a molecular formula of  $C_{21}H_{24}N_{8.2}HCl$ , 11 g/L water solubility at 25 °C, and thermal stability, was used as the synthetic wastewater source. A 1000 ppm dye solution was prepared as a stock aqueous solution, and the aqueous stream was auxiliary diluted as needed. The Fenton reagent oxidation system for *Saccharum officinarum* was initiated using  $H_2O_2$  as the peroxide reagent source (30% w/v, provided by Sigma-Aldrich, Darmstadt, Germany). The pH of the aqueous dye stream was adjusted to the required values using Sigma-Aldrich's  $H_2SO_4$  or NaOH as needed. All chemicals were used as received from the supplier, without any additional treatment.

## 2.2. *Saccharum Officinarum* Activation and Preparation

Sampling expeditions were conducted to obtain *Saccharum officinarum* residuals from a sugarcane refinery located in the southern region of Egypt, where it is extensively grown. The dried and milled *Saccharum officinarum* powder was thoroughly washed repeatedly before being dried overnight in an electric oven at 105 °C to eliminate any remaining moisture. Then, the obtained material was subjected to chemical treatment described in the literature [26,27], as follows: It was soaked for 2 h in an alkali (1 N NaOH). While being soaked, it was heated and stirred. Then, the soaked material was washed multiple times with distilled water until it reached a neutral pH, when the washing water was disposed of. The resultant blend was then subjected to 1 h of stirring with sulfuric acid under heating. After separation and drying, the material was ball milled for size reduction prior to pyrolysis at 500 °C. The material was thus activated and ready for use.

## 2.3. Bench Scale Set-up

To investigate the impact of dye loading on photo-catalytic oxidation, a glass vessel was filled with 100 mL of wastewater effluent containing Bismarck Brown dye. A stock solution of 1000 ppm dye was prepared and then diluted to the required concentrations (5, 10, 20, and 40 ppm) as per the experimental conditions. Subsequently, *Saccharum officinarum* ranging from 20 to 80 mg/L and H<sub>2</sub>O<sub>2</sub> ranging from 100 to 800 mg/L were added to the aqueous stream as a source of Fenton's reagent. To ensure proper catalyst dispersion, the solution was sonicated for 5 min. An ultraviolet lamp (15 W, 230 V/50 Hz) emitting UV illumination of a specific wavelength (253.7 nm) was employed to initiate the photo-catalytic reaction. The lamp was covered with a silica tube jacket to shield it from the aqueous solution and then submerged in the solution. The solution temperature and pH were adjusted as required before the catalyst was added. To carry out the oxidation experiment, the dye solution containing the reagents was subjected to UV irradiance. The sleeved UV lamp was placed inside the aqueous solution to ensure UV irradiance while the solution was magnetically stirred during the reaction time, which led to the oxidation process. Next, at specific time intervals (each 10 min), samples were withdrawn for analysis. Each sample was first passed through a micro-filter for catalyst separation. Finally, the *Saccharum officinarum* substance was removed through settling and washed repeatedly and the substrate was filtered for cyclic use.

The Bismarck Brown dye removal performance was computed using the following relation:

$$\zeta(\%) = \frac{C_0 - C_t}{C_0} \times 100 \quad (1)$$

where

$\zeta(\%)$  is the Bismarck Brown dye removal performance and  $C_0$  and  $C_t$  are the initial dye concentration and the final (postoxidation) dye concentration, respectively.

In addition, the data plotted against time are the values of  $C_t/C_0$  [28]. Figure 1 presents a graphical illustration of the experiment.

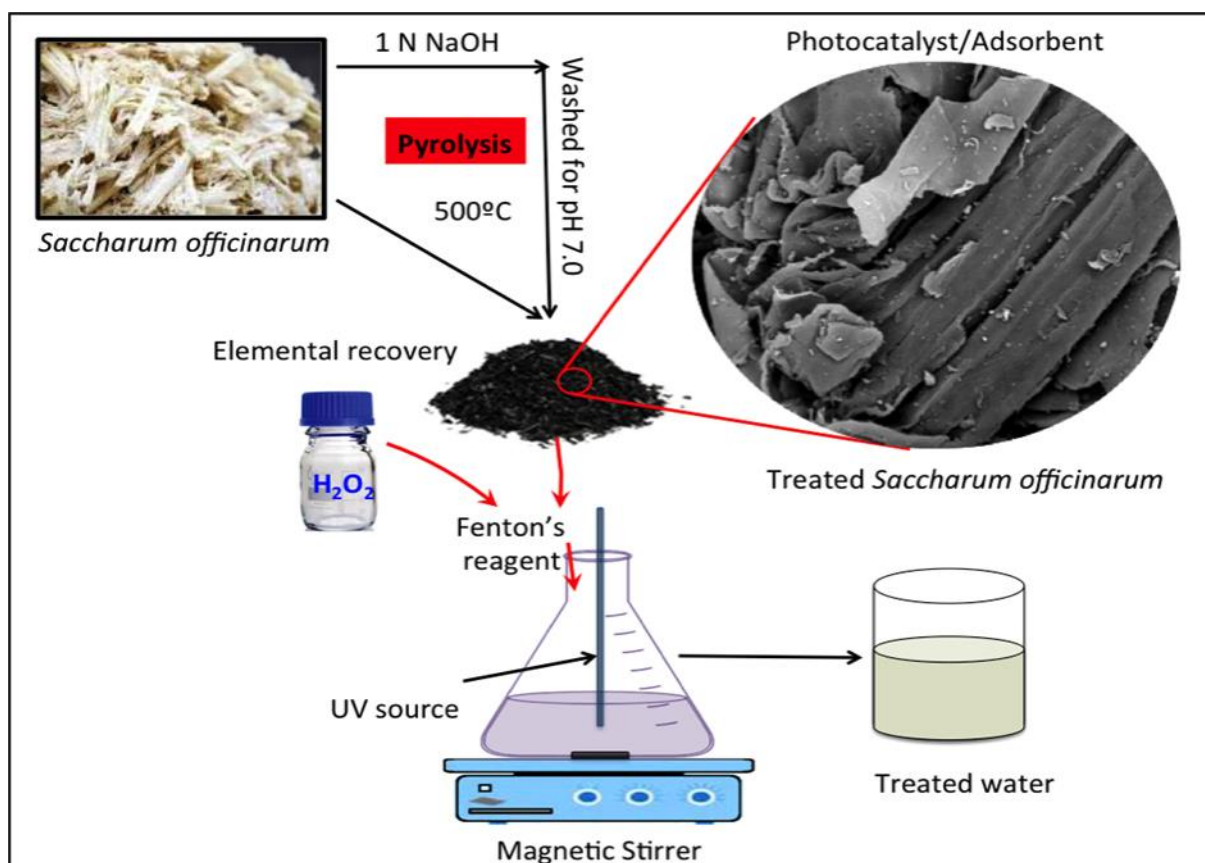


**Figure 1.** Graphical representation of the catalyst preparation and photocatalytic treatment steps.

#### 2.4. Analytical Determination

To determine the extent of Bismarck Brown dye removal and oxidation, UV–Vis analysis was performed using a Unico UV-2100 spectrophotometer, USA, that investigated at the maximum wavelength of the dye ( $\lambda$  526 nm), which represents the maximum absorbance peak. The pH of the Bismarck Brown dye aqueous effluent was monitored and adjusted through a digital pH instrument (AD1030, Adwa company, Szeged, Hungary).

#### 2.5. Catalyst Characterization

The X-ray diffraction (XRD) analysis of the crystallinity of the chemically and thermally prepared *Saccharum officinarum* material, as well as native *Saccharum officinarum* material, was conducted using a Bruker-Nonius Kappa CCD diffractometer with a  $CuK\alpha$  radiation source at a wavelength of  $\lambda = 1.5406 \text{ \AA}$  in step-scanned mode for 18.87 s. The diffractometer machine operated at 45 kV. The micro-structure morphology of *Saccharum officinarum* was explored using scanning electron micrographs (SEMs) obtained from a field-emission scanning electron microscope (FE-SEM), Quanta FEG 250, with typical magnifications of  $\times 8000$  and  $\times 60,000$ . The analysis was complemented with energy-dispersive X-ray spectroscopy (EDX) to analyze the principal oxides.

#### 2.6. Experimental Design

A three-level factorial design (Box–Behnken model) with triplicates of central values was used to understand the effect of independent variables on the dependent parameter of Bismarck Brown dye oxidation (%). The independent parameters selected, on the basis of their influence on the process, were pH value, *Saccharum officinarum*, and  $H_2O_2$  dose. The level of each Box–Behnken factor was determined on the basis of preliminary experiments and is presented in Table 1.

**Table 1.** Coded and un-coded levels of the selected independent variables used in Box–Behnken factorial design.

Selected Parameters	Symbol		Codified Levels		
			Low	Medium	High
	Un-Coded	Coded	−1	0	1
pH	$E_1$	$\varepsilon_1$	2	3	4
<i>Saccharum officinarum</i> dose (mg/L)	$E_2$	$\varepsilon_2$	30	40	50
Hydrogen peroxide (mg/L)	$E_3$	$\varepsilon_3$	350	400	450

The full factorial experimental design matrix was generated using statistical analysis software (SAS, Institute, New York, NY 10019, USA). Statistical and graphical analyses were performed using SAS and Matlab (7.11.0.584), respectively. The adequacy of the proposed statistical model was assessed using the analysis of variance (ANOVA) test. A second-order polynomial model was employed to establish the relationship among Bismarck Brown dye oxidation rate (%), the dependent parameter, and the operating independent variables. The corresponding quadratic equation is presented as Equation (2).

$$\zeta = \beta_0 + \sum \beta_o \varepsilon_i + \sum \beta_{ii} \varepsilon_i^2 + \sum \sum \beta_{ij} \varepsilon_i \varepsilon_j \quad (2)$$

where

$\zeta$  is the projected (suggested by the model) dye oxidation removal rate dependent variable response (%);  $i = 1, 2, 3$ , and  $j = 1, 2, 3$ ;  $\beta_0$ ,  $\beta_i$ ,  $\beta_{ii}$ , and  $\beta_{ij}$  are the design regression coefficient variables;

and  $\varepsilon_i$  is the input controlling coded variable.

To simplify the proposed design calculations, the un-coded parameters of the operating system ( $E_i$ ) were assigned to coded variables ( $\varepsilon_i$ ) in accordance with Equation (2). In addition, after the model significance, the optimum values were calculated through Mathematica software (V 5.2). Then, three additional experiments were carried out at the optimal predicted values to validate the predicted model.

### 3. Results and Discussions

#### 3.1. Structural and Morphological Characterization of *Saccharum officinarum*

##### 3.1.1. XRD Analysis

X-ray diffraction analysis was performed to investigate and evaluate the mineralogical composition of pure and treated *Saccharum officinarum* material, and the data are represented in Figure 2. The pattern displays the characteristics of the mineral. The XRD analysis shows that in terms of mineralogical composition, *Saccharum officinarum* consists of a bundle of minerals, and not only one mineral, as indicated by the various peaks for each mineral [12,29]. Various oxides identified in the XRD pattern of the treated *Saccharum officinarum* are Na<sub>2</sub>O, SiO<sub>2</sub>, CaO, MgO, Al<sub>2</sub>O<sub>3</sub>, and Fe<sub>2</sub>O<sub>3</sub> (Figure 2b). The peaks at 2 $\theta$  of 32.4, 37.1, and 43.1 indicate the occurrence of CaO [30,31]. In addition, the existence of quartz (SiO<sub>2</sub>) is signified by the peaks of 21.0, 21.4, 27.1, 37.2, 39.5, and 44.9 [32]. Na<sub>2</sub>O is specified by the 2 $\theta$  value of 37.8.

Further, Fe<sub>2</sub>O<sub>3</sub> can be identified from the 2 $\theta$  value of 24.4. Al<sub>2</sub>O<sub>3</sub> is located at the peaks of 33.3, 37.2, and 43.1 [33]. The pure *Saccharum officinarum* displayed in Figure 2a shows the existence of SiO<sub>2</sub>, CaO, and Al<sub>2</sub>O<sub>3</sub> in lesser amounts than in the treated *Saccharum officinarum*. It is noteworthy to mention that other oxides, such as Na<sub>2</sub>O, MgO, and Fe<sub>2</sub>O<sub>3</sub>, did not appear in the native sample. The disappearance of the amorphous nature is also indicated in the treated material.

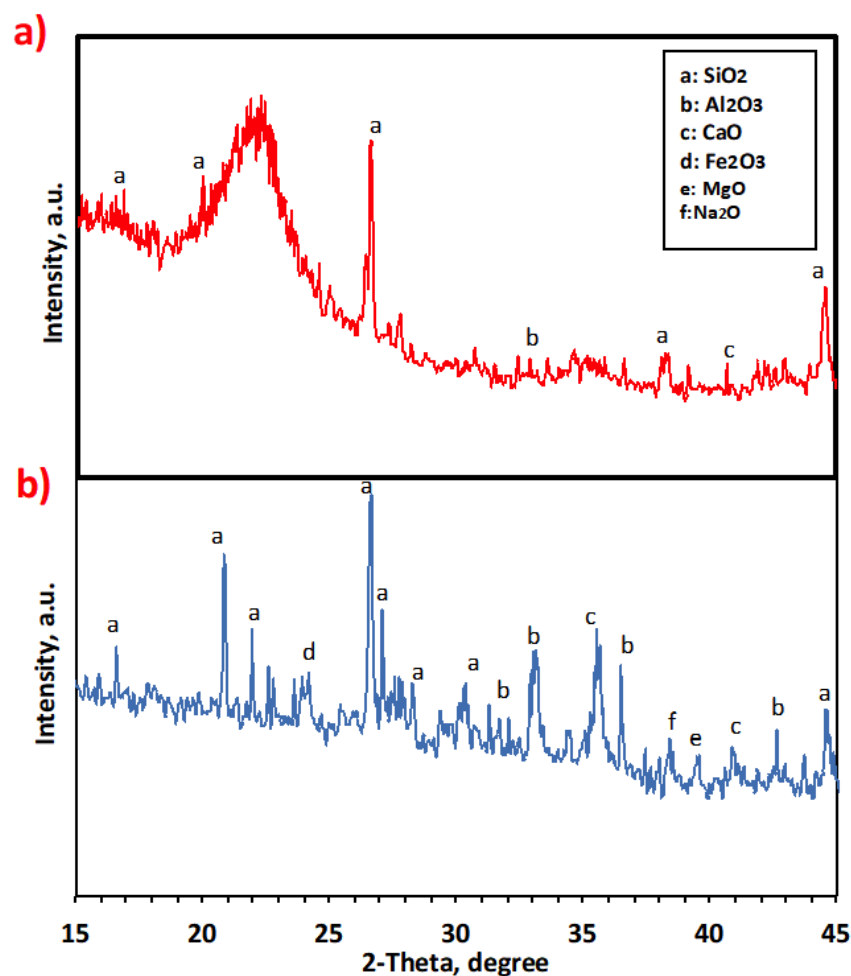


Figure 2. XRD pattern of the prepared *Saccharum officinarum*: (a) pure *Saccharum officinarum* and (b) modified *Saccharum officinarum*.

The significant increase in the cellulose content in the chemically treated sample is the reason behind the increased cellulose crystallinity. However, such behavior is not observed in the untreated sample, as shown in Figure 2a, due to the occurrence of high amounts of lignin, which might cover the outer space of the cellulose structure [34]. Additionally, chemical–thermal treatments lead to decomposition reactions, which produce some oxides, in accordance with Cordeiro et al. [35].

Table 2 presents the EDX analysis of the arrangement of the elements in *Saccharum officinarum*, showing its elemental composition. The major elements present are CaO, SiO<sub>2</sub>, Al<sub>2</sub>O<sub>3</sub>, Fe<sub>2</sub>O<sub>3</sub>, MgO, Na<sub>2</sub>O, and MnO. The occurrence of considerable amounts of Fe<sub>2</sub>O<sub>3</sub>, Al<sub>2</sub>O<sub>3</sub>, MnO, and MgO, indicated by the XRD analysis, confirms the source of metals before Fenton’s reaction. The waste-derived catalyst with a high elemental content, which reflects good catalytic activity along with other active factors, can essentially catalyze the oxidation reaction.

Table 2. Chemical composition of *Saccharum officinarum* calcined at 500 °C as inferred by EDX.

Element	CaO	SiO <sub>2</sub>	Al <sub>2</sub> O <sub>3</sub>	Fe <sub>2</sub> O <sub>3</sub>	MgO	Na <sub>2</sub> O	MnO	L.O.I.
Weight %	15.54	57.10	8.40	9.62	1.58	0.46	3.64	4.13

Although Fe<sup>2+/3+</sup> promotes Fenton’s reaction, other oxides, such as MnO<sub>2</sub> [36,37] and Al<sub>2</sub>O<sub>3</sub> [38], display catalytic activity for active Fenton-like reaction. Hence, the presence of such oxides in the modified *Saccharum officinarum* promotes Fenton’s reaction. Furthermore,

due to the waste iron sludge produced after Fenton's treatment and for easier separation and reusability, research has focused on heterogeneous Fenton catalysts. In this regard, a variety of supports, such as SiO<sub>2</sub> and various clay materials, have been introduced to improve the catalytic performance of Fenton's reaction. Furthermore, MgO has previously exhibited to be an excellent adsorbent [39]. In addition, Silva et al. [40] coupled Cu and MgO to promote Fenton's reaction.

### 3.1.2. SEM Imaging

The morphology of *Saccharum officinarum* was evaluated from FE-SEM images. These images show different morphologies because of the effect of chemical–thermal activation, with particles of different shapes. Scanning electron micrographs of pure *Saccharum officinarum* and treated material are displayed in Figure 3.

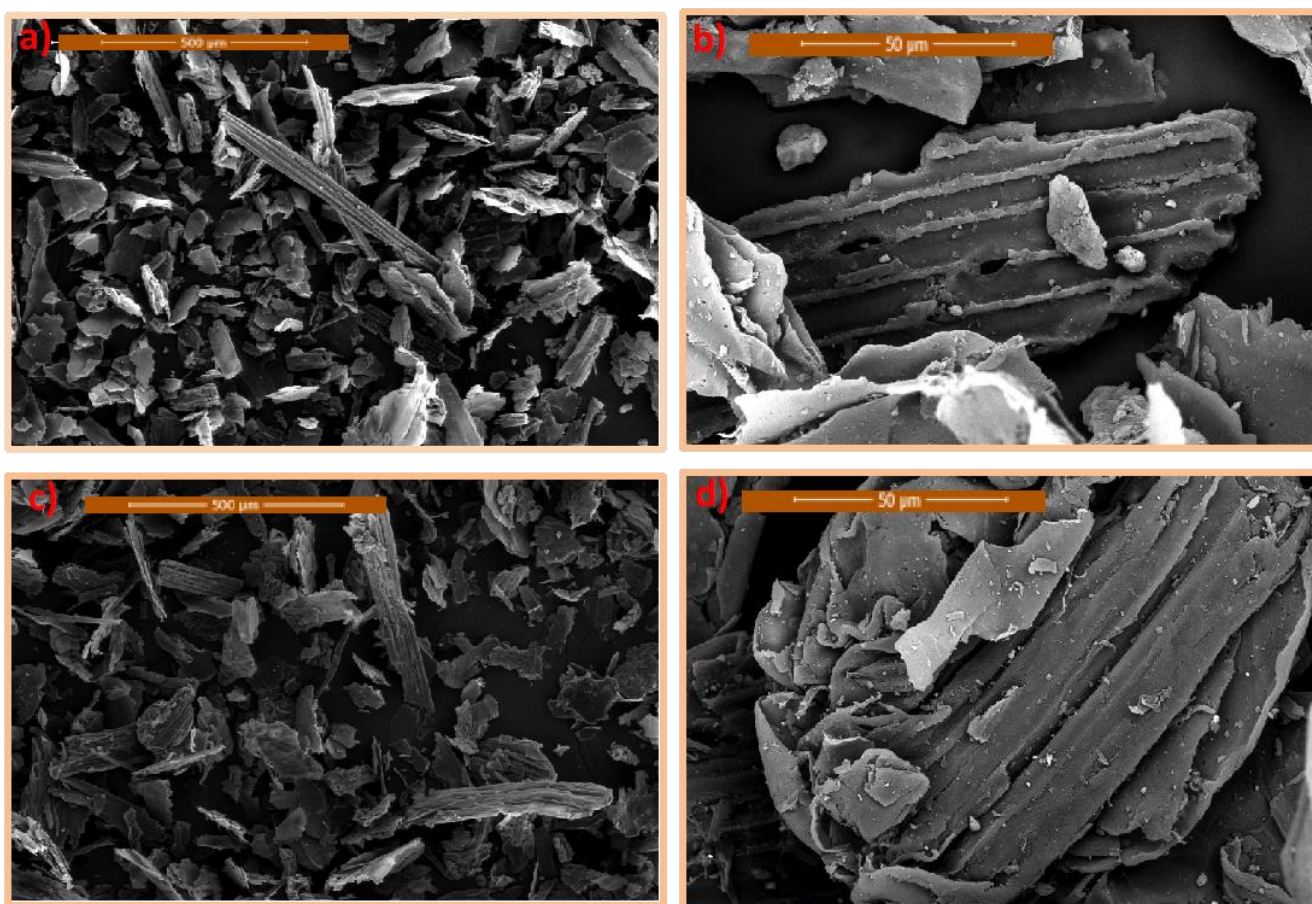


**Figure 3.** Scanning electron microscope (SEM) images of pure native (a,b) and treated *Saccharum officinarum* (c,d) at different magnifications.

Figure 3a,b explores pure *Saccharum officinarum* at different magnifications, displaying slightly organized particles of a heterogeneous size and shape. Such pure *Saccharum officinarum* material morphology shows a severely compact structure. However, the morphology of treated samples, in Figure 3c,d, shows noticeable differences. The chemically modified *Saccharum officinarum* surface shows a disturbance in the cell wall structure, with reduced adherence between the cells. Such alteration would increase the surface area of the catalyst surface, which will lead to extra availability for catalytic reaction. At a high magnification (Figure 3d), the thermally and chemically modified sample displays a high degree of disorganization of particles, with lower fiber adhesion in comparison to that in Figure 2b (prior to treatment). Furthermore, the specific surface area of *Saccharum officinarum* is monitored and recorded at 436 g/m<sup>2</sup>.

### 3.2. Dye Oxidation by the Modified Oxidation System

#### 3.2.1. Optimum Reaction Time and Comparative Investigation

Different treatment processes (the adsorption system involving the *Saccharum officinarum* substance; *Saccharum officinarum*/H<sub>2</sub>O<sub>2</sub> under UV illumination, called the photo-Fenton system; and *Saccharum officinarum*/H<sub>2</sub>O<sub>2</sub>, called the dark Fenton system) for the treatment of Bismarck Brown dye in wastewater are compared. Fenton's reagent concentrations were *Saccharum officinarum* = 40 mg/L and H<sub>2</sub>O<sub>2</sub> = 800 mg/L at the initial pH of 3.0. For all systems, the essential illumination time to reach the plateau state was explored, as shown in Figure 4.

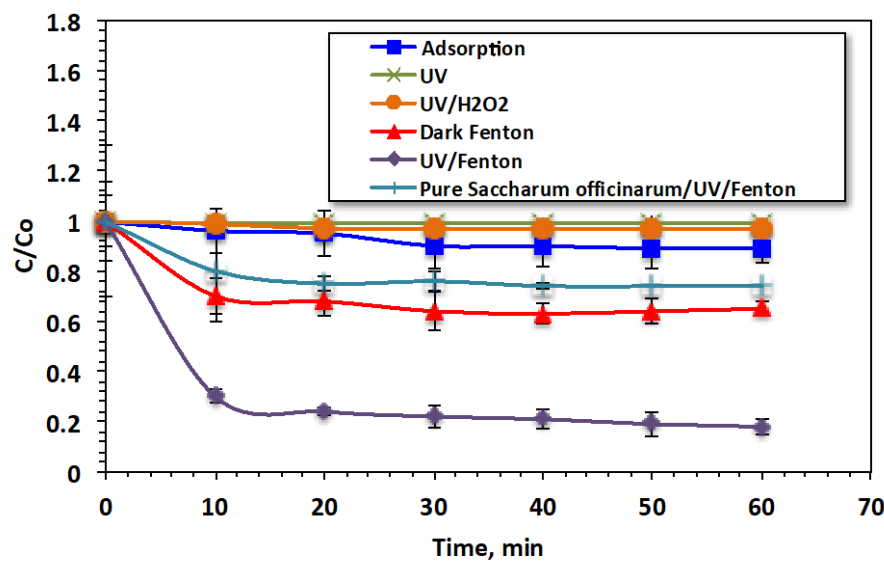


Figure 4. Bismarck Brown dye oxidation through various systems.

The data presented in Figure 4 indicate that the adsorption system had the lowest removal efficiency. The photo-oxidation system under UV illumination was more effective than the dark oxidation system. The data reveal that using *Saccharum officinarum* alone for treatment led to the removal of only 11% of the Bismarck Brown dye after 60 min of contact time. However, when Fenton's reagent was added in the dark, the removal efficiency increased to 35%. When H<sub>2</sub>O<sub>2</sub> was added to the wastewater under UV illumination, the removal efficiency increased significantly, to 82%, demonstrating the effectiveness of the Fenton oxidation reaction. The ·OH radicals generated during treatment with Fenton's were sufficient for attacking the dye molecules and converting them into harmless end products (CO<sub>2</sub> and H<sub>2</sub>O). UV illumination in combination with Fenton's reagent demonstrated a pronounced removal effect, possibly due to the additional reaction intermediates, ·OH radicals, generated by the UV illumination. These findings agree with previous studies mentioned in the literature [41]. Furthermore, to verify the role of *Saccharum officinarum*, treatment using UV/H<sub>2</sub>O<sub>2</sub> at a dose of H<sub>2</sub>O<sub>2</sub> of 400 mg/L is carried out. According to the experimental data, only 3% of the dye is oxidized by using the solo hydrogen peroxide system. The data confirm the role of *Saccharum officinarum* and the effectiveness of Fenton's reaction. This means that the production of ·OH radicals is limited compared to those generated from Fenton's reaction. Furthermore, solo UV irradiance is applied, which removes only 1% of the dye. However, no Fenton's reaction occurred in the case of the unmodified *Saccharum officinarum* since the oxidation efficiency is lower than that of UV/H<sub>2</sub>O<sub>2</sub> treatment (only 26%). This treatment effect could be due to the hydrogen peroxide and UV, which are the main factors responsible for oxidation. However, the presence of untreated *Saccharum officinarum* renders the reaction since it is shadowing the UV light instead of leading to Fenton's reaction. These results agree with the previous findings of Samet et al. [42] in treating insecticide-containing wastewater through Fenton's system.



### 3.2.2. Effect of Initial Dye Loading

Figure 5 illustrates the influence of various loads of Bismarck Brown dye on oxidation efficiency. Figure 5 shows that the dye oxidation efficiency (70%) was supreme when the starting dye load was the minimum (5 ppm) after 10 min of illumination time and steadily reduced thereafter, achieving an accumulative oxidation efficacy of 92% in 60 min. As previously mentioned, Bismarck Brown dye molecules are made of aromatic rings.  $\cdot\text{OH}$  species, produced by the reaction between metals of Fenton's reaction and  $\text{H}_2\text{O}_2$ , attack such rings and open them, resulting in the formation of reaction intermediates and oxidizing them into the harmless  $\text{CO}_2$  and  $\text{H}_2\text{O}$ . This could be attributed to the fact that as the reaction proceeds, the concentration of  $\cdot\text{OH}$  radicals produced gradually declines due to the reduction in  $\text{H}_2\text{O}_2$  concentration. Additionally, radicals other than hydroxyl radicals are generated that hinder the Bismarck Brown dye oxidation rate instead of increasing it. An examination of Figure 5 reveals the rapid degradation of the dye removal attained in the initial time period and a reduction in the oxidation rate with an increase in the dye load. The oxidation efficacies are 92, 78, 74, and 72% for dye concentrations of 5, 10, 20, and 40 ppm in the wastewater, respectively. This is because the generated  $\cdot\text{OH}$  species are inadequate for treating the whole dye. Increasing the oxidation activity, under UV illumination, by reducing the starting pollutant load has previously been investigated in [41], where the authors applied Fenton's oxidation to treat benzimidazole. Although the oxidation varies for various concentrations, the same trend is observed in the high initial drop in concentration followed by a slower oxidation rate in all cases. This phenomenon is associated with the hydrogen peroxide consumption as the reaction proceeds. This reagent plays a vital role in the generation of hydroxyl radicals, which is the main responsibility of the oxidation reaction [28].

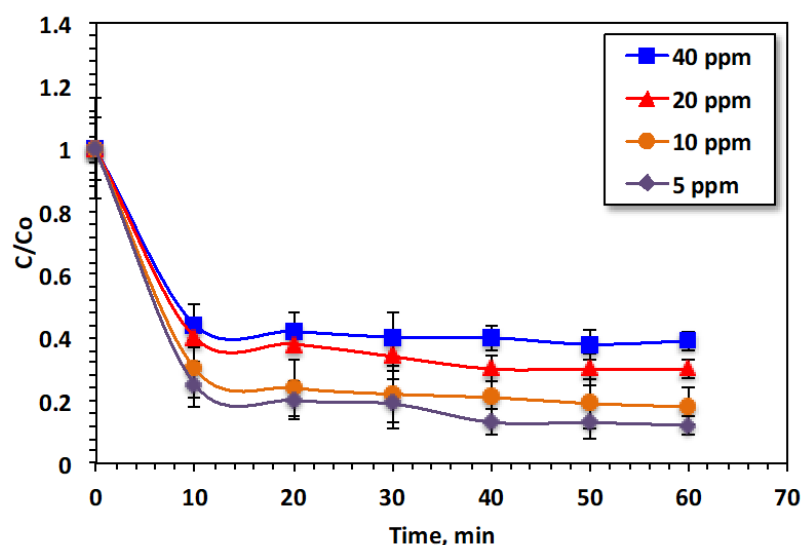


Figure 5. Influence of Bismarck Brown dye loading on the oxidation effectiveness.

### 3.2.3. Effect of Modified Fenton Variables

#### Effect of *Saccharum officinarum* Dose

To examine the influence of *Saccharum officinarum* particles on the treatment of Bismarck Brown dye by Fenton's reaction, experiments were conducted to explore the effect of *Saccharum officinarum* concentration on reaction kinetics. Figure 6a displays the influence of *Saccharum officinarum* on the oxidation system when the *Saccharum officinarum* dose is varied over a range of 10 to 80 mg/L. The oxidation efficacy elevated from 39% to 82% when the *Saccharum officinarum* dose increased from 10 to 40 mg/L. However, on further increase in the concentration of *Saccharum officinarum*, to 80 mg/L, the oxidation efficacy decreased significantly, to 30%. Elements such as aluminum, iron, and manganese, which act as the source of Fenton's reaction, are critical for initiating the production of the photoactive metal

hydroxo intermediate complexes that absorb the photons in the UV illumination and thus generate the  $\cdot\text{OH}$  species. Such non-selective  $\cdot\text{OH}$  species attack the dye particles, further oxidizing and mineralizing them.

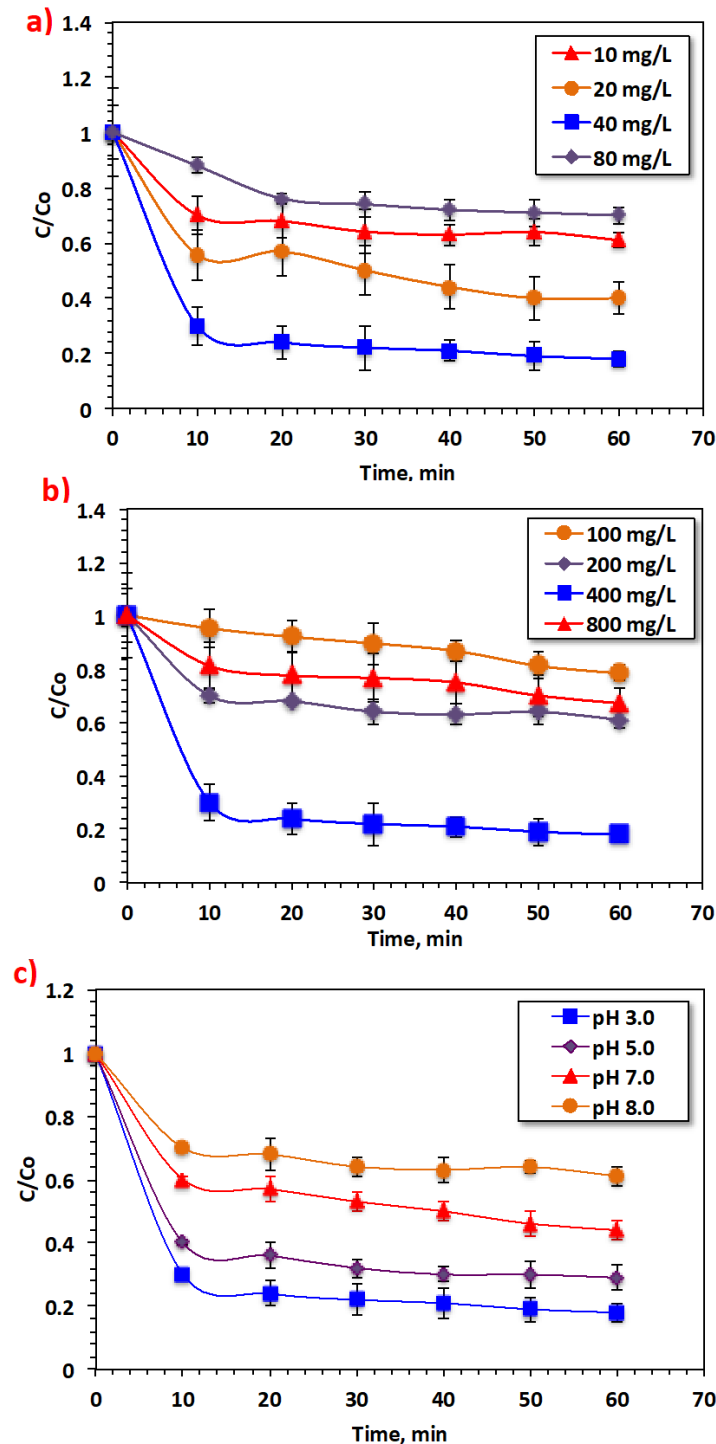


**Figure 6.** Effect of modified Fenton's reaction parameters on the oxidation of Bismarck Brown dye: (a) *Saccharum officinarum* dose; (b) H<sub>2</sub>O<sub>2</sub> dose; (c) pH value.

An elevation in *Saccharum officinarum* reagent to a dose of 40 mg/L increases oxidation efficiency. However, excessive *Saccharum officinarum* particles in the reaction medium hinder the elements that produce  $\cdot\text{OH}$  radicals [43]. In addition, at higher metal concentrations, a muddy, highly colored, aqueous solution is generated, reducing the diffusion of the ultraviolet

light into the aqueous wastewater stream. Therefore, hydrogen peroxide reagent photolysis, producing the hydroxyl radicals, is hindered. Hence, an excess of *Saccharum officinarum* in the solution of Fenton's reaction results in reduced dye removal efficiency. Shende [44] previously verified this by treating violet dye contained in wastewater.

#### Effect of Hydrogen Peroxide Reagent Dose

Figure 6b displays the effect of the  $H_2O_2$  dose on the oxidation of Bismarck Brown dye molecules in dye-comprising aqueous media. As estimated, elevating the peroxide dose from 100 to 400 mg/L improved the dye oxidation rate and the removal efficacy was enhanced from 21% to 82%. This increase in the removal rate is associated with the extra  $\cdot OH$  radicals produced through hydrogen peroxide decomposition. However, an excessive increase in the dose of this reagent (higher than 400 mg/L) does not further improve dye removal. For example, increasing the  $H_2O_2$  dosage to 800 mg/L led to a decline in dye removal, to only 32%. Obviously, excessive  $H_2O_2$  concentration hinders the production of the highly reactive  $\cdot OH$  radicals, generating the less reactive perhydroxyl radicals ( $HO_2\cdot$ ) in the reaction medium instead. Such radicals cause a decline in the reaction rate due to the insignificant oxidation capabilities. Therefore, the optimal operating  $H_2O_2$  dose, corresponding to the maximum dye removal, was recorded at 400 mg/L. Various authors [45–47] have previously highlighted that Fenton's reaction might occur at an optimal hydrogen peroxide dose.

#### Starting pH Effectiveness

Wastewater pH is a vital factor in Fenton's system. Taking this into consideration, the starting pH value for the aqueous solution was altered over the range of 3.0 to 8.0 since it shows a role in  $H_2O_2$  decay and the hydrolytic speciation of the metal ions. The data displayed in Figure 6c reveal that the dye removal efficacy is highly correlated with the starting solution pH value and the optimal pH is recorded at 3.0. Unsurprisingly, the removal efficiency increases to 82% and declines with further pH increase. Moreover, increasing the alkalinity of the solution results in further reduction in the dye removal efficiency, to 39%. This might be because the fraction of soluble metal ions declines considerably with pH elevation. In addition, inactive hydroperoxide ( $HO_2\cdot$ ) radicals are formed in the oxidation medium, hindering the oxidation rate [48].

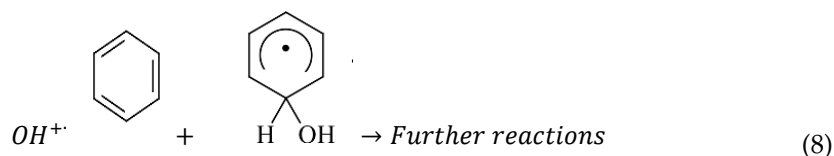
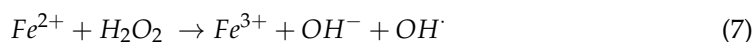
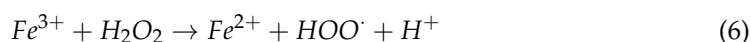
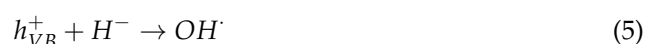
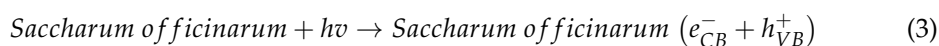
Contrarily, an acidic pH value leads to extra  $H^+$  ions in the reaction medium that react with the superoxide. This reaction leads to a reduction in the elements present in the *Saccharum officinarum* residuals and the dissolved  $O_2$ . The result is the formation of hydroperoxide ( $HO_2\cdot$ ), an inactive radical. The overall reaction is inhibited due to the presence of hydroperoxide radical ( $HO_2\cdot$ ) and the superoxide radical anion ( $O_2\cdot^-$ ), categorized as scavenger radicals, in the reaction medium [48]. This might lead to a decline in the Bismarck Brown oxidation yield, which further declines at alkaline pH conditions since *Saccharum officinarum* significantly reduces at pH of about 8.

#### Oxidation Mechanism

An arbitrary mixture composed of several metals originating from *Saccharum officinarum* leads to additive series reduction in oxidation (Red-OX) reactions. Such reactions lead to the production of oxidizing species. Under UV illumination, several metals on *Saccharum officinarum* are irradiated and an electron (e)/hole (h) pair is produced on the surface of *Saccharum officinarum*, which is the reaction media (Equation (3)). This photo-induced hole might react with  $H_2O$  in the solution to generate  $\cdot OH$  species, as illustrated in Equations (4) and (5). Furthermore, hydrogen peroxide could react with the metal ions present in *Saccharum officinarum*, such as iron, to induce Fenton's reaction, producing extra hydroxyl radicals, as given in Equations (6) and (7) [49,50]. The molecules of Bismarck Brown dye, a type of azo dye, have an aromatic type of structure. The highly reactive hydroxyl radicals produced in the aqueous media attack the aromatic ring in the Bismarck Brown dye molecules in order to hydroxylase them by generating a chain of hydroxycyclohexadienyl radicals to mineralize the dye (Equation (8)). Such

hydroxylation reaction is mainly responsible for the steady conversion of aromatic compounds into  $\text{CO}_2$ . Moreover, hydroxyl radicals and the  $\text{H}^+$  in the solution react to produce water, which is the end product (Equation (9)).

Although  $\text{H}_2\text{O}_2$  promotes the generation of  $\cdot\text{OH}$  radicals, its presence in higher doses reduces the oxidation reaction efficiency. This is due to the extra peroxide competing with the dye to react with the  $\cdot\text{OH}$ , resulting in a scavenging effect on the overall reaction rate. Moreover, the two identical hydroxyl radicals recombine and inhibit the overall reaction rate (Equations (10) and (11)) [51].



### 3.3. Regression Model Fitting and ANOVA Testing

The performance of the three independent critical factors, pH value, and *Saccharum officinarum* concentrations on the modified Fenton oxidation of Bismarck Brown dye was simulated and assessed after 10 min of illumination irradiance time, using RSM based on Box–Behnken experimental design. The experimental design matrix suggested by the software was carried out, and the quadratic polynomial design equation exhibited the related response role according to the following equation:

$$\zeta(\%) = 55.46 - 0.26 \varepsilon_1 - 3.401\varepsilon_2 + 1.4\varepsilon_3 - 25.02\varepsilon_1^2 + 0.51\varepsilon_1\varepsilon_2 + 16.11\varepsilon_1\varepsilon_3 - 17.41\varepsilon_2^2 + 2.80\varepsilon_2\varepsilon_3 - 8.1\varepsilon_3^2 \quad (12)$$

ANOVA analysis based on Fisher's statistical examination for ANOVA analysis (Table 3) was carried out to assess the statistical consequence and the adequacy of the proposed polynomial quadratic design. The quadratic model was found to be the best fit when it possesses a small standard deviation with a minimal probability value ( $<0.005$ ) and a high regression coefficient ( $R^2$ ). The  $R^2$ -value for the Bismarck brown dye removal response was 96%, with a small probability ( $p$ ) value. This confirms a high relationship between the predicted values based on the quadratic design model and the experimental values.

**Table 3.** Estimates of the model regression for Bismarck Brown dye removal under *Saccharum officinarum*–Fenton oxidation \*.

Source of Variation	Degrees of Freedom	Sum of Squares	Mean Square	F-Value	p-Value
Regression	9	9	4744.6348	4744.6348	88.601959
Linear	3	3	106.75	106.75	1.993464
Quadratic	3	3	3263.981	3263.981	60.952024
Cross product	3	3	1373.9038	1373.9038	25.656471
Error	5	4647.6			
Lack of fit	3	4379.85	486.65	9.087768	0.012817
Pure error	2	267.75	53.55		
Total	14	4647.6			

\*  $R^2 = 96\%$ ;  $Adj-R^2 = 87\%$ .

The Matlab software (version, 7.11.0.584) was used to generate 3D surface and 2D contour plots of the parameters. Figures 7–9 illustrate the response of each experimental parameter and the main interactions between the investigated variables. Inspection of the 3D surface graph and 2D contour plots of Figure 7a,b indicates that the rate of oxidation of the dye increases with increasing *Saccharum officinarum* concentration. Meanwhile, the curvature displayed in Figure 7a illustrates the significant influence of the interaction between catalyst dose and pH value. Such good interaction leads to the high yield of hydroxyl radicals, which enhance the dye oxidation rate, as shown by the contour plot of Figure 7a. However, a further increase in the reagent dose reduces the oxidation efficiency.

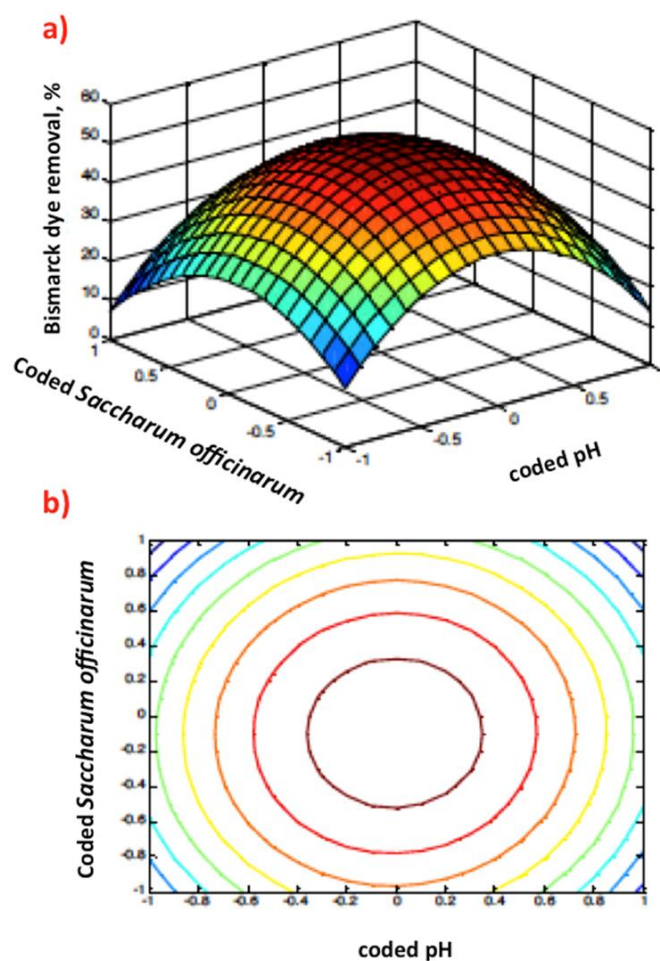
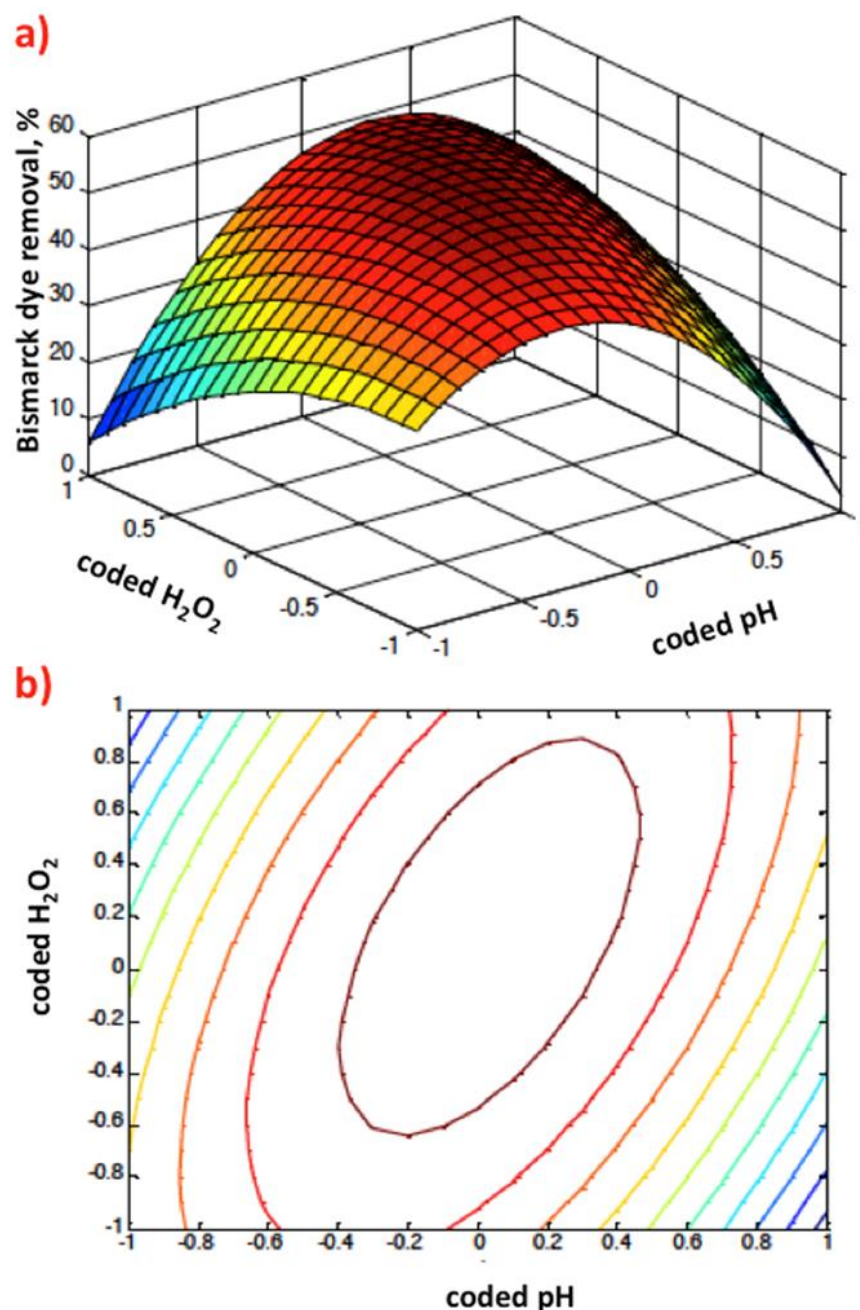
**Figure 7.** Graphical representation of the Box–Behnken response 3D surface (a) and 2D (b) contour plots of coded pH value and *Saccharum officinarum* dose.

Figure 8a,b demonstrates via 3D response surface and contour plots the influence of *Saccharum officinarum* dose and pH. The graphical representation scheme verifies that the oxidation rates were enhanced with increasing the *Saccharum officinarum* dose. In addition, the acidic environment is favorable for dye oxidation and thus the optimum pH is in the acidic range. This could be explained by the existence of unfavorable radicals in the reaction aqueous solution media as the pH value increases, hindering the reaction rate.



**Figure 8.** Graphical representation of Box–Behnken response 3D surface (a) and 2D (b) contour plots of coded pH value and hydrogen peroxide dose.

Though the optimal pH of the aqueous solution is close to the acidic pH, this is still considered an obstacle for real application. It is worth mentioning that conversion of waste to wealth is the main advantage of the suggested modified system.

Figure 9a,b illustrates the relation of the coded values of *Saccharum officinarum* and hydrogen peroxide for dye oxidation. The 3D response surface and contour plots indicate

that an increase in independent variables increases the removal efficiency. The surface and contour plots of the design display that the highest percentage of Bismarck Brown dye oxidation was attained at the junction near the origin of the two parameters. This investigation confirms the relation between reagent doses and the generation of  $\cdot\text{OH}$  radicals. This oxidation methodology is highly cost efficient since it is based on a waste-originated catalyst.

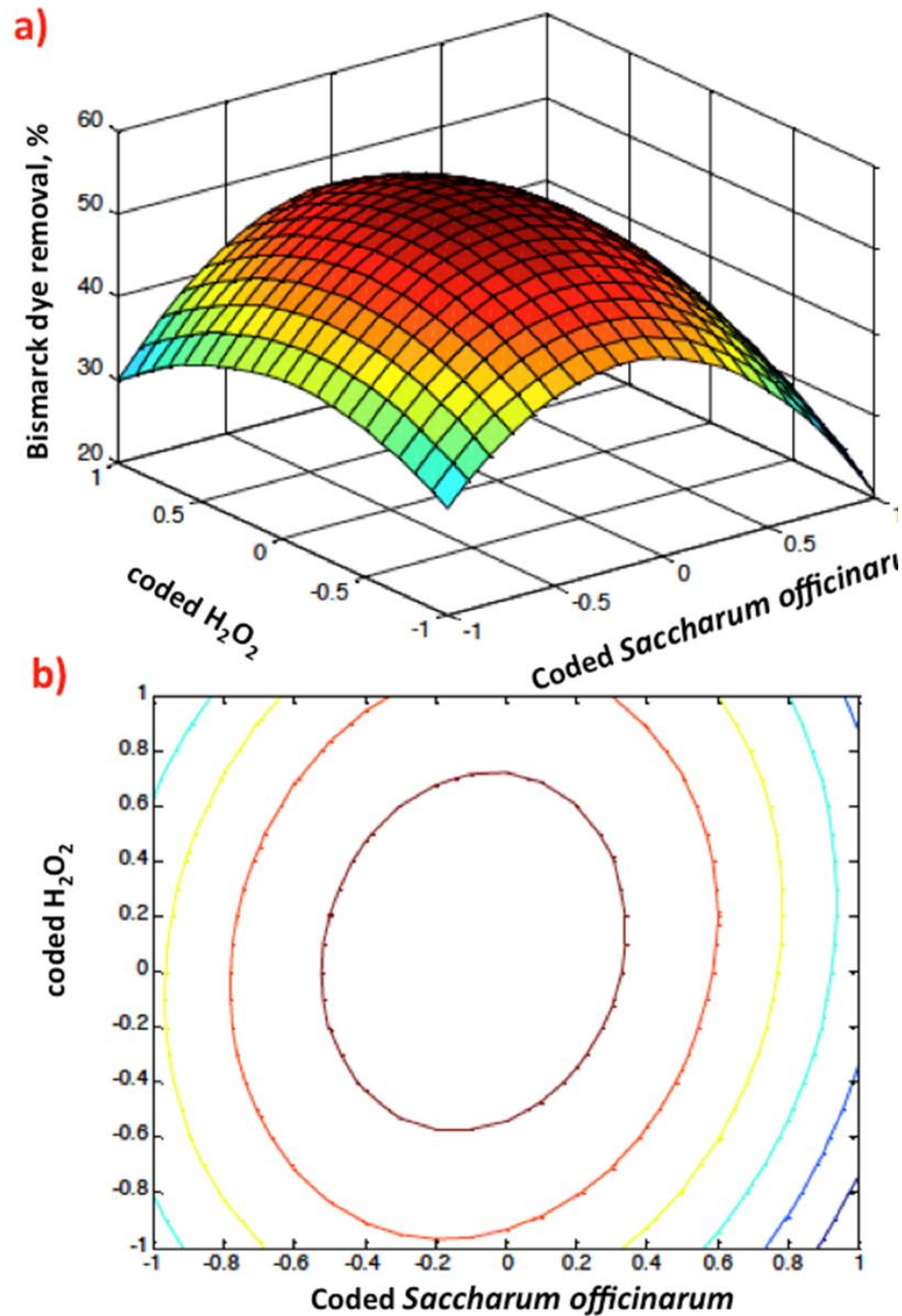


**Figure 9.** Graphical representation of Box–Behnken response 3D surface (a) and 2D (b) contour plots of coded *Saccharum officinarum* and hydrogen peroxide dose.

To check the adequacy of the suggested model, the statistically suggested optimized predicted variables (pH 2.9, *Saccharum officinarum* at 39 mg/L, and  $\text{H}_2\text{O}_2$  at 402 mg/L)

were used to conduct three replicates of the experiments. After 10 min of reaction time, the predicted percentage of dye removal reached 54%. After another 10 min, the experimental values reached 55% and with the preceding experiment, the final reduction achieved was 85%, compared to 82% when manually optimized values are used.

This investigation verifies the significance of the RSM in optimizing the operating parameters that influence Bismarck Brown dye oxidation using modified Fenton's reaction via *Saccharum officinarum* particles as a waste material.

### 3.4. Temperature Effect

In this part of the study, the oxidation kinetics and thermodynamics of Bismarck Brown dye oxidation are examined. The investigation is based on the kinetics of the photo-oxidation of Bismarck Brown by a modified photo-Fenton system based on *Saccharum officinarum* particles under a constant concentration at working temperatures of 32, 40, 50, and 60 °C.

The data in Figure 10 display the positive impact of elevating the operating temperature on dye removal. Temperature elevation completes the reaction more efficiently. The oxidation efficacy improves from 82% to 90% as the temperature increases from 32 to 60 °C, probably because of the excellent production of hydroxyl radicals at high temperatures [48] because of collisions between the dye particles in the aqueous medium. Moreover, temperature increase affects the reaction between H<sub>2</sub>O<sub>2</sub> and metal ions originating from *Saccharum officinarum*, increasing the ·OH output rate and accelerating Fenton's reaction, leading to increased dye oxidation in the form of color removal [52].

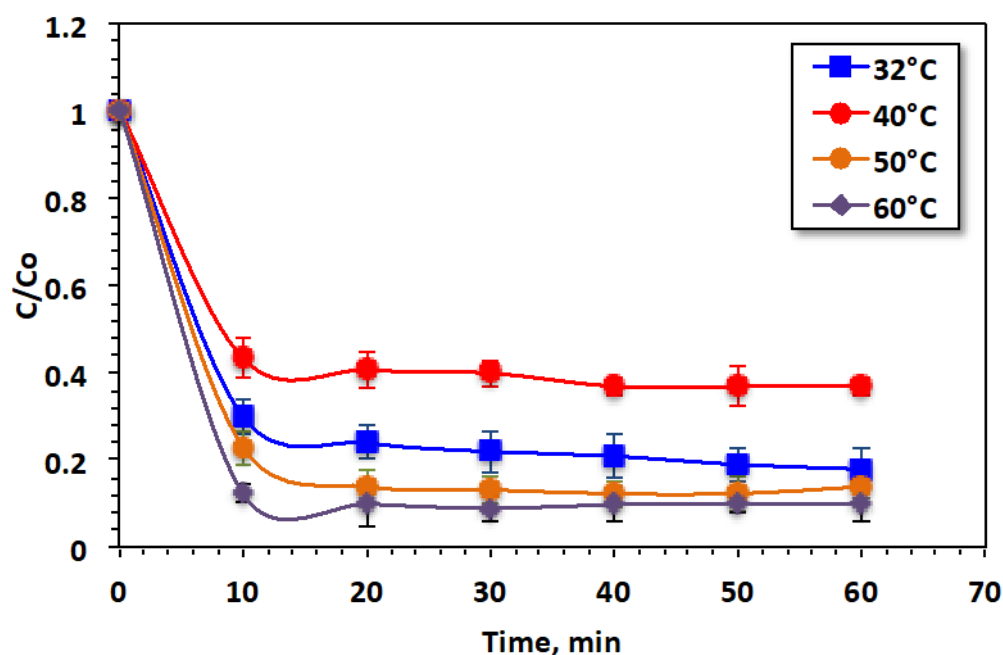


**Figure 10.** Effect of temperature on Bismarck Brown dye removal by the modified *Saccharum officinarum*–Fenton process.

### 3.5. Kinetics and Thermodynamic Investigation

To further understand the modified Fenton's reaction, the kinetics rates of first- and second-order reactions were investigated in accordance with the oxidation of Bismarck Brown via the photo-Fenton treatment system based on *Saccharum officinarum* particles. Such kinetic rate orders have been explained by the linearized form of such orders as displayed in Equations (13) and (14) for the first- and second-order reactions, respectively [28,29].

$$C_t = C_0 - e^{k_1 t} \quad (13)$$



$$\left(\frac{1}{C_t}\right) = \left(\frac{1}{C_0}\right) - k_2t \tag{14}$$

where  $C_0$  and  $C_t$  are the doses of Bismarck Brown dye initially and at time  $t$ , respectively, and  $k_1$  and  $k_2$  represent the kinetic rate constants of first- and second-order reaction kinetics, respectively.

By plotting Equations (13) and (14), the most appropriate reaction kinetics for the experimental data suitable for Bismarck Brown dye removal were investigated (Figure 11). Table 4 displays kinetic parameters for each kinetic order and also their corresponding  $R^2$  values of the regression coefficients.

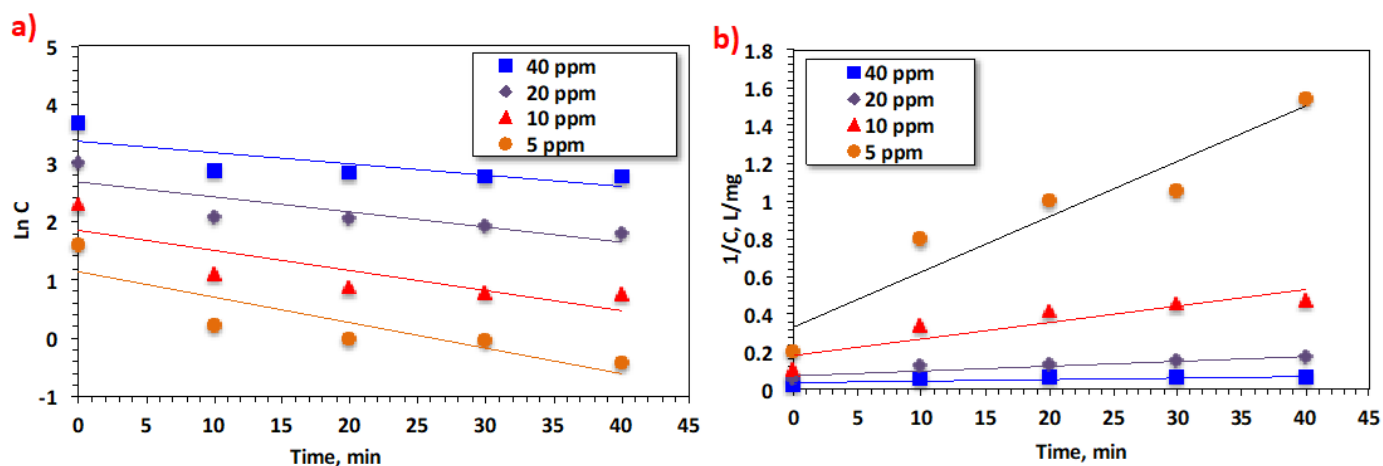


**Figure 11.** Effectiveness of temperature on Bismarck Brown dye oxidation by the *Saccharum officinarum*–Fenton process.

**Table 4.** Kinetic parameters of Bismarck Brown dye oxidation by a photo-Fenton reagent based on *Saccharum officinarum* under different concentrations.

Concentration, ppm	First-Order Reaction Kinetics			Second-Order Reaction Kinetics		
	$k_1$ , min <sup>-1</sup>	R <sup>2</sup>	$t_{1/2}$ , min	$k_2$ , L.mg <sup>-1</sup> min <sup>-1</sup>	R <sup>2</sup>	$t_{1/2}$ , min
5	0.0193	0.59	35.9067	0.0293	0.95	170.64021
10	0.0257	0.72	26.9649	0.0087	0.90	1149.4212
20	0.0343	0.69	20.2040	0.0026	0.92	7692.3101
40	0.0435	0.77	15.9310	0.0008	0.70	50,000.0001

Based on the  $R^2$  values, the appropriate kinetic model is selected representing the data for investigating the kinetic order. To locate the best fit, the data exhibited in Table 4 from this investigation signifies that the first model is rejected because it has lower  $R^2$  values (ranging from 0.59 to 0.77). The correlation values are quite high for the second-order kinetic model, ranging from 0.70 to 0.95. Thus, the second-order model has the greatest correlation coefficient. In this regard, Fenton’s system in the current form generally follows second-order kinetics. Furthermore, the lowest value of half-life time ( $t_{1/2}$ ) corresponds to the lower dye concentration. Such records agree with those listed in the literature [42]. However, other studies have investigated Fenton’s reaction following the first-order kinetic reaction rate.

The kinetic constants investigated for the second-order model treatment processes of this model range from 0.0008 to 0.0293 mg<sup>-1</sup> L min<sup>-1</sup>. This slight difference in the  $K_2$  values is related to the concentration load, which affects the oxidation intermediates and the dye removal rate in the aqueous medium. As tabulated in Table 4, the half-life time ( $t_{1/2}$ ) increases as the initial dye concentration increases. This might be attributed to the fact that increasing the dye concentration hinders the catalytic activity of *Saccharum officinarum*

to adsorb Bismarck Brown dye since the *Saccharum officinarum* surface is saturated with Bismarck Brown molecules. In addition, the  $\cdot\text{OH}$  output oxidants are not sufficient for oxidizing Bismarck Brown at too-high concentrations [53].

To understand the reaction for real applications, thermodynamic parametric values were calculated for a photo-Fenton oxidation system based on *Saccharum officinarum*. The activation energy ( $E_a$ ) of the Brown dye oxidation can be calculated [54] by using the Arrhenius equation revelation equation for the kinetic rate constant,  $k_2 = Ae^{-\frac{E_a}{RT}}$ , where  $R$  is the universal gas constant value ( $8.314 \text{ J mol}^{-1}\text{K}^{-1}$ ),  $T$  is the reaction temperature in kelvin quantity, and  $A$  is the pre-exponential constant. Then, taking the natural log of the Arrhenius formula and plotting  $\ln k_2$  versus  $1000/T$  (Figure 12), a straight-line relationship is achieved where its slope could be used to calculate  $E_a$  (energy of activation). The activation energy of the system was recorded at  $64.43 \text{ kJ mol}^{-1}$ .

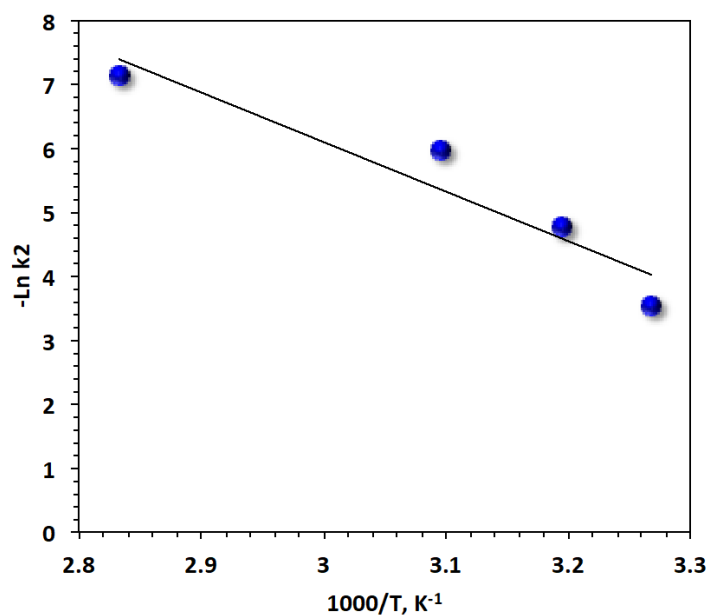


**Figure 12.** Plot of  $\ln k_2$  versus  $1000/T$  for Bismarck Brown dye removal by the modified *Saccharum officinarum*–Fenton process (solid lines represent least-squares fitting).

Table 5 displays the other thermodynamic parameters, such as the enthalpy of activation ( $\Delta H' = E_a - RT$ ), the entropy of activation ( $\Delta S' = (\Delta H' - \Delta G')/T$ ), and the free energy of activation ( $\Delta G'$ ) that was projected using Eyring's equation ( $k_2 = \frac{k_B T}{h} e^{(-\frac{\Delta G'}{RT})}$ ), where  $k_B$  and  $h$  are Boltzmann and Planck's constant, respectively [45]. Table 5 exhibits  $\Delta H'$  (within the temperature range) values in a positive range, indicating that the reaction is endothermic. In addition,  $\Delta G'$  shows positive values, indicating that the system is non-spontaneous at high temperatures with a negative entropy of activation. This result might be due to the development of a well-solvated structure between the dye molecules and  $\cdot\text{OH}$  species.

**Table 5.** Thermodynamic variables of Bismarck Brown oxidation by a photo-Fenton reagent based on modified *Saccharum officinarum*.

Temperature, K	$E_a$ , $\text{kJmol}^{-1}$	$\Delta G'$ , $\text{kJmol}^{-1}$	$\Delta H'$ , $\text{kJmol}^{-1}$	$\Delta S'$ , $\text{Jmol}^{-1}$
306	64.43	83.98	61.88	−72.24
313		89.12	61.82	−87.24
323		95.30	61.74	−103.91
353		107.87	61.49	−131.40

### 3.6. Catalyst Reusability

The reusability of *Saccharum officinarum* catalyst, in terms of sustainability, is investigated by identifying its oxidation affinity after cyclic use. Initially, *Saccharum officinarum*, which is collected after each cycle, is subjected to three sequential washing with distilled water, filtered, and oven-dried at 105 °C for 1 h [55,56]. Then, the catalyst is subjected to successive cycles for dye oxidation and the data are exhibited in Figure 13.

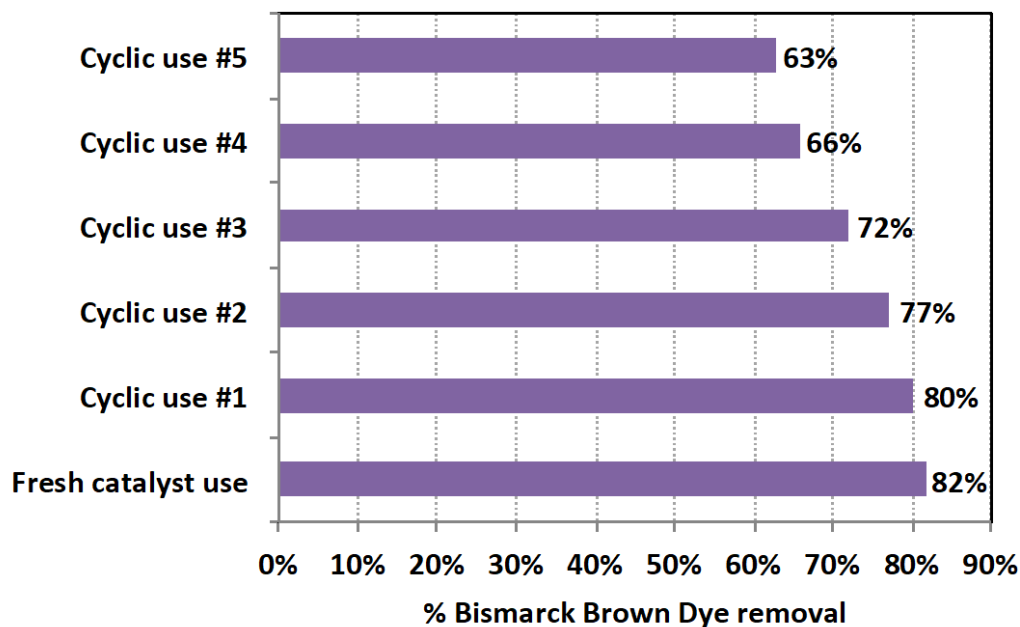


Figure 13. Bismarck Brown dye oxidation in the modified *Saccharum officinarum* system in consecutive cycles.

As shown in Figure 13, as the catalyst is used multiple times, its activity declines, as indicated by its oxidation efficiency. Compared to the oxidation efficiency of 82% when fresh catalyst is used, by the fifth cyclic use, its oxidation efficiency is reduced to 63%. In addition, the catalytic activity is reduced after each use as indicated by the decline in the removal efficiency, as seen in Figure 13. This might be attributed to the fact that pollutant intermediates cover the active centers of the catalyst, preventing them from attacking contaminants in wastewater. Hence, the overall reaction rate is reduced. It is worth mentioning the activity of the material is still high.

## 4. Conclusions

A modified Fenton system based on a combination of metals originating from *Saccharum officinarum* bio-waste as the source of Fenton's catalyst can act as a superior economical oxidation system. Chemical–thermal-treated *Saccharum officinarum* was augmented with hydrogen peroxide and applied for treating simulated wastewater loaded with the textile dye named Bismarck Brown dye. *Saccharum officinarum* was characterized, and various metals were found in the modified material. *Saccharum officinarum* exhibited multifunctional treatment activity, showing high efficiency in terms of Bismarck Brown dye oxidation and mineralization. Bismarck Brown dye was oxidized within 60 min of irradiance time. The response surface methodology was applied to optimize the system for dye oxidation. The highest dye removal was achieved by using the optimized operational conditions of 39 and 402 mg/L of *Saccharum officinarum* and H<sub>2</sub>O<sub>2</sub> reagents, respectively, in an acidic pH medium. In addition, the operating parameters were optimized and the kinetics of the reaction were examined. The kinetic data revealed that the reaction follows second-order reaction kinetics with a global activation energy of 64.43 kJ/mol. The reaction is endothermic and non-spontaneous in nature. Moreover, it was confirmed

that *Saccharum officinarum* can be recovered to be recycled, indicating its sustainability as a catalyst since it could oxidize the dye solution till the fifth cyclic use. Hence, the system can be a promising technique for eliminating textile dyeing discharge effluents.

**Author Contributions:** Conceptualization, E.A.H. and M.A.T.; methodology, E.A.H., M.A.T., H.A.N. and M.M.A.; software, H.A.N. and M.M.A.; validation, E.A.H. and M.A.T.; investigation, E.A.H., M.A.T., H.A.N. and M.M.A.; resources E.A.H., M.A.T., H.A.N. and M.M.A.; writing—original draft preparation, E.A.H., M.A.T., H.A.N. and M.M.A.; writing—review and editing, E.A.H., M.A.T., H.A.N. and M.M.A.; project administration E.A.H. All authors have read and agreed to the published version of the manuscript.

**Funding:** Prince Sattam bin Abdulaziz University for funding this research work through project number (PSAU/2023/01/23018).

**Data Availability Statement:** Data available upon request.

**Acknowledgments:** The authors extend their appreciation to Prince Sattam bin Abdulaziz University for funding this research work through project number (PSAU/2023/01/23018).

**Conflicts of Interest:** The authors declare no conflict of interest.

## References

- Pirsaheb, M.; Moradi, S.; Shahlaei, M.; Wang, X.; Farhadian, N. A new composite of nano zero-valent iron encapsulated in carbon dots for oxidative removal of bio-refractory antibiotics from water. *J. Clean. Prod.* **2019**, *209*, 1523–1532. [\[CrossRef\]](#)
- Ng, W.P.Q.; Lam, H.L.; Ng, F.Y.; Kamal, M.; Lim, J.H.E. Waste-to-wealth: Green potential from palm biomass in Malaysia. *J. Clean. Prod.* **2012**, *34*, 57–65. [\[CrossRef\]](#)
- Gu, L.; Zhu, N.; Guo, H.; Huang, S.; Lou, Z.; Yuan, H. Adsorption and Fenton-like degradation of naphthalene dye intermediate on sewage sludge derived porous carbon. *J. Hazard. Mater.* **2013**, *246*, 145–153. [\[CrossRef\]](#)
- Ullah, T.; Gul, H.; Khitab, F.; Khattak, R.; Ali, Y.; Rasool, S.; Khan, M.S.; Zekker, I. Adsorption of Remazol Brilliant Violet-5R from Aqueous Solution Using Sugarcane Bagasse as Biosorbent: Kinetic and Thermodynamic Studies. *Water* **2022**, *14*, 3014. [\[CrossRef\]](#)
- Petchwattana, N.; Naknaen, P.; Narupai, B. A circular economy use of waste wood sawdust for wood plastic composite production: Effect of bio-plasticiser on the toughness. *Int. J. Sustain. Eng.* **2020**, *13*, 398–410. [\[CrossRef\]](#)
- Betiku, E.; Etim, A.O.; Pereao, O.; Ojumu, T.V. Two-step conversion of neem (*Azadirachta indica*) seed oil into fatty methyl esters using heterogeneous biomass based catalyst: An example of cocoa pod husk. *Energy Fuels* **2017**, *31*, 6182–6193. [\[CrossRef\]](#)
- Nath, B.; Das, B.; Kalita, P.; Basumatary, S. Waste to value addition: Utilization of waste Brassica nigra plant derived novel green heterogeneous base catalyst for effective synthesis of biodiesel. *J. Clean. Prod.* **2019**, *239*, 118112. [\[CrossRef\]](#)
- Sun, N.; Wen, X.; Yan, C. Adsorption of mercury ions from wastewater aqueous solution by amide functionalized cellulose from sugarcane bagasse. *Int. J. Biol. Macromol.* **2018**, *108*, 1199. [\[CrossRef\]](#)
- Ahamad, T.; Ruksana, M.N.; Alhabarah, A.N.; Alshehri, A. N/S doped highly porous magnetic carbon aerogel derived from sugarcane bagasse cellulose for the removal of bisphenol-A. *Int. J. Biol. Macromol.* **2019**, *132*, 1031. [\[CrossRef\]](#)
- Xiong, W.; Zhang, J.; Yu, J.; Chi, R. Selective removal from aqueous solution on phosphoric acid modified sugarcane bagasse fixed-bed column. *Process. Saf. Environ.* **2019**, *124*, 75–83. [\[CrossRef\]](#)
- Wu, J.; Ding, T.; Sun, J. Neurotoxic potential of iron oxide nanoparticles in the rat brain striatum and hippocampus. *Neurotoxicology* **2013**, *34*, 243–253. [\[CrossRef\]](#) [\[PubMed\]](#)
- Gupta, C.K.; Sachan, A.K.; Kumar, R. Examination of Microstructure of Sugar Cane Bagasse Ash and Sugar Cane Bagasse Ash Blended Cement Mortar. *Sugar Tech.* **2021**, *23*, 651–660. [\[CrossRef\]](#)
- Tireli, A.A.; Guimarães, I.D.R.; Terra, J.C.D.S.; da Silva, R.R.; Guerreiro, M.C. Fenton-like processes and adsorption using iron oxide-pillared clay with magnetic properties for organic compound mitigation. *Environ. Sci. Pollut. Res.* **2015**, *22*, 870–881. [\[CrossRef\]](#)
- Pathak, G.; Das, D.; Rajkumari, K.; Rokhum, S.L. Exploiting waste: Towards a sustainable production of biodiesel using Musa acuminata peel ash as a heterogeneous catalyst. *Green Chem.* **2018**, *20*, 2365–2373. [\[CrossRef\]](#)
- Velichkova, F.; Julcour-Lebigue, C.; Koumanova, B.; Delmas, H. Heterogeneous Fenton oxidation of paracetamol using iron oxide (nano) particles. *J. Environ. Chem. Eng.* **2013**, *1*, 1214–1222. [\[CrossRef\]](#)
- Van, H.T.; Nguyen, L.H.; Hoang, T.K.; Nguyen, T.T.; Tran, T.N.H.; Nguyen, T.B.H.; Vu, X.H.; Pham, M.T.; Tran, T.P.; Pham, T.T.; et al. Heterogeneous Fenton oxidation of paracetamol in aqueous solution using iron slag as a catalyst: Degradation mechanisms and kinetics. *Environ. Technol. Innov.* **2020**, *18*, 100670. [\[CrossRef\]](#)
- Valdez, H.A.; Jiménez, G.G.; Granados, S.G.; de León, C.P. Degradation of paracetamol by advance oxidation processes using modified reticulated vitreous carbon electrodes with TiO<sub>2</sub> and CuO/TiO<sub>2</sub>/Al<sub>2</sub>O<sub>3</sub>. *Chemosphere* **2012**, *89*, 1195–1201. [\[CrossRef\]](#)
- Tinti, A.; Tugnoli, V.; Bonora, S.; Francioso, O. Recent applications of vibrational mid-Infrared (IR) spectroscopy for studying soil components: A review. *J. Cent. Eur. Agric.* **2015**, *16*, 1–22. [\[CrossRef\]](#)

19. Bao, T.; Jin, J.; Damtie, M.M.; Wu, K.; Yu, Z.M.; Wang, L.; Chen, J.; Zhang, Y.; Frost, R.L. Green synthesis and application of nanoscale zero-valent iron/rectorite composite material for P-chlorophenol degradation via heterogeneous Fenton reaction. *J. Saudi Chem. Soc.* **2019**, *23*, 864–878. [[CrossRef](#)]
20. Nassar, M.Y.; Abdelrahman, E.A. Hydrothermal tuning of the morphology and crystallite size of zeolite nanostructures for simultaneous adsorption and photocatalytic degradation of methylene blue dye. *J. Mol. Liq.* **2017**, *242*, 364–374. [[CrossRef](#)]
21. Betiku, E.; Ajala, S.O. Modeling and optimization of Thevetia peruviana (yellowoleander) oil biodiesel synthesis via Musa paradisical (plantain) peels as heterogeneous base catalyst: A case of artificial neural network vs. response surface methodology. *Ind. Crop. Prod.* **2014**, *53*, 314–322. [[CrossRef](#)]
22. Mendonça, I.M.; Paes, O.A.; Maia, P.J.; Souza, M.P.; Almeida, R.A.; Silva, C.C.; Duvoisin, S., Jr.; de Freitas, F.A. New heterogeneous catalyst for biodiesel production from waste tucum~a peels (*Astrocaryum aculeatum* Meyer): Parameters optimization study. *Renew. Energy* **2019**, *130*, 103–110. [[CrossRef](#)]
23. Gopinath, S.; Kumar, P.V.; Kumar, P.S.M.; Arafath, K.Y.; Sivanesan, S.; Baskaralingam, P. Cs-tungstosilicic acid/Zr-KIT-6 for esterification of oleic acid and transesterification of non-edible oils for green diesel production. *Fuel* **2018**, *234*, 824–835. [[CrossRef](#)]
24. Zhang, M.H.; Dong, H.; Zhao, L.; Wang, D.X.; Meng, D. A review on Fenton process for organic wastewater treatment based on optimization perspective. *Sci. Total Environ.* **2019**, *670*, 110–121. [[CrossRef](#)] [[PubMed](#)]
25. Holkar, C.R.; Jadhav, A.J.; Pinjari, D.V.; Mahamuni, N.M.; Pandit, A.B. A critical review on textile wastewater treatments: Possible approaches. *J. Environ. Manag.* **2016**, *182*, 351–366. [[CrossRef](#)] [[PubMed](#)]
26. Rezende, C.A.; De Lima, M.A.; Maziero, P.; de Azevedo, E.R.; Garcia, W.; Polikarpov, I. Chemical and morphological characterization of sugarcane bagasse submitted to a delignification process for enhanced enzymatic digestibility. *Biotechnol. Biofuels* **2011**, *4*, 54. [[CrossRef](#)] [[PubMed](#)]
27. Abdel-Halim, E.S. Chemical modification of cellulose extracted from sugarcane bagasse: Preparation of hydroxyethyl cellulose. *Arab. J. Chem.* **2014**, *7*, 362–371. [[CrossRef](#)]
28. Thabet, R.H.; Tony, M.A.; El Sherbiny, S.A.; Ali, I.A.; Fouad, M.K. Catalytic oxidation over nanostructured heterogeneous process as an effective tool for environmental remediation. In Proceedings of the IOP Conference Series: Materials Science and Engineering, Cairo, Egypt, 7–9 April 2020; IOP Publishing: Bristol, UK, 2020; Volume 975, p. 012004.
29. Demir, I.; Güzelkücük, S.; Sevim, Ö.; Filazi, A.; Şengül, Ç.G. Examination of microstructure of fly ash in cement. *Int. Adv. Mech. Civ. Eng.* **2017**, *5*, 49–51.
30. Basumatary, B.; Das, B.; Nath, B.; Basumatary, S. Synthesis and characterization of heterogeneous catalyst from sugarcane bagasse: Production of jatropha seed oil methyl esters. *Curr. Res. Green Sustain. Chem.* **2021**, *4*, 100082. [[CrossRef](#)]
31. Fan, M.; Wu, H.; Shi, M.; Zhang, P.; Jiang, P. Well-dispersive K<sub>2</sub>O-KCl alkaline catalyst derived from waste banana peel for biodiesel synthesis. *Green Energy Environ.* **2019**, *4*, 322–327. [[CrossRef](#)]
32. Faria, K.C.P.; Gurgel, R.F.; Holanda, J.N.F. Recycling of sugarcane bagasse ash waste in the production of clay bricks. *J. Environ. Manag.* **2012**, *101*, 7–12. [[CrossRef](#)]
33. Schettino, M.A.S.; Holanda, J.N.F. Characterization of sugarcane bagasse ash waste for its use in ceramic floor tile. *Procedia Mater. Sci.* **2015**, *8*, 190–196. [[CrossRef](#)]
34. El Oudiani, A.; Chaabouni, Y.; Msahli, S.; Sakli, F. Crystal transition from cellulose I to cellulose II in NaOH treated *Agave americana* L. fibre. *Carbohydr. Polym.* **2011**, *86*, 1221–1229. [[CrossRef](#)]
35. Cordeiro, G.C.; Toledo Filho, R.D.; Fairbairn, E.M.R. Effect of calcination temperature on the pozzolanic activity of sugar cane bagasse ash. *Constr. Build. Mater.* **2009**, *23*, 3301–3303. [[CrossRef](#)]
36. Ou, J.; Tian, H.; Wu, J.; Gao, J.; Jiang, J.; Liu, K.; Wang, S.; Wang, F.; Tong, F.; Ye, Y.; et al. MnO<sub>2</sub>-Based Nanomotors with Active Fenton-like Mn<sup>2+</sup> Delivery for Enhanced Chemodynamic Therapy. *ACS Appl. Mater. Interfaces* **2021**, *13*, 38050–38060. [[CrossRef](#)] [[PubMed](#)]
37. Cao, W.; Jin, M.; Yang, K.; Chen, B.; Xiong, M.; Li, X.; Cao, G. Fenton/Fenton-like metal-based nanomaterials combine with oxidase for synergistic tumor therapy. *J. Nanobiotechnol.* **2021**, *19*, 325. [[CrossRef](#)]
38. Wei, X.; Wu, H.; Sun, F. Magnetite/Fe-Al-montmorillonite as a Fenton catalyst with efficient degradation of phenol. *J. Colloid Interface Sci.* **2017**, *504*, 611–619. [[CrossRef](#)]
39. Silva, M.; Murzin, V.; Zhang, L.; Baltrus, J.; Baltrusaitis, J. Transition metal doped MgO nanoparticles for nutrient recycling: An alternate Mg source for struvite synthesis from wastewater. *Environ. Sci. Nano* **2020**, *7*, 3482–3496. [[CrossRef](#)]
40. Silva, M.; Eisa, M.; Ragauskaitė, D.; McMinn, M.H.; Tian, Z.; Williams, C.; Knopf, A.; Zhang, L.; Baltrusaitis, J. Treatment of emerging contaminants in simulated wastewater via tandem photo-Fenton-like reaction and nutrient recovery. *Environ. Sci. Water Res. Technol.* **2023**, *9*, 508–522. [[CrossRef](#)]
41. Liu, Q.; Qian, K.; Qi, J.; Li, C.; Yao, C.; Song, W.; Wang, Y. Improving the efficiency of Fenton reactions and their application in the degradation of benzimidazole in wastewater. *RSC Adv.* **2018**, *8*, 9741–9748. [[CrossRef](#)] [[PubMed](#)]
42. Samet, Y.; Hmani, E.; Abdelhedi, R. Fenton and solar photo-Fenton processes for the removal of chlorpyrifos insecticide in wastewater. *Water SA* **2012**, *38*, 537–542. [[CrossRef](#)]
43. Rodriguez-Chueca, J.; Polo-Lopez, M.I.; Mosteo, R.; Ormad, M.P.; Fernandez-Ibanez, P. Disinfection of real and simulated urban wastewater effluents using a mild solar photo-Fenton. *Appl. Catal. B* **2014**, *150–151*, 619–629. [[CrossRef](#)]

44. Shende, T.; Bhanvase, B.; Rathod, A.; Pinjari, D.; Sonawane, S. Sonochemical synthesis of Graphene-Ce-TiO<sub>2</sub> and Graphene-Fe-TiO<sub>2</sub> ternary hybrid photocatalyst nanocomposite and its application in degradation of Crystal Violet Dye. *Ultrason. Sonochem.* **2018**, *41*, 582–589. [[CrossRef](#)]
45. Bounab, L.; Iglesias, O.; Gonzalez-Romero, E.; Pazos, M.; Sanroman, M.A. Effective heterogeneous electro-Fenton process of m-cresol with iron loaded activated carbon. *RSC Adv.* **2015**, *5*, 31049–31056. [[CrossRef](#)]
46. El Haddad, M.; Regti, A.; Laamari, M.R.; Mamouni, R.; Saffaj, N. Use of Fenton reagent as advanced oxidative process for removing textile dyes from aqueous solutions. *J. Mater. Environ. Sci.* **2014**, *5*, 667–674.
47. Daniela, A.; Andrea, N.; Berkovic, M.; Costante Maria, M.R.; Juliarena, P.; Fernando, S.; Einschlag, G. Nitrobenzene degradation in Fenton-like systems using Cu(II) as catalyst. Comparison between Cu(II)- and Fe(III)-based systems. *Chem. Eng. J.* **2013**, *228*, 1148–1157.
48. Thabet, R.H.; Fouad, M.K.; Ali, I.A.; El Sherbiney, S.A.; Tony, M.A. Magnetite-based nanoparticles as an efficient hybrid heterogeneous adsorption/oxidation process for reactive textile dye removal from wastewater matrix. *Inter. J. Environ. Anal. Chem.* **2021**. [[CrossRef](#)]
49. Ramirez, J.H.; Maldonado-Hódar, F.J.; Pérez-Cadenas, A.F.; Moreno-Castilla, C.; Costa, C.A.; Madeira, L.M. Azo-dye Orange II degradation by heterogeneous Fenton-like reaction using carbon-Fe catalysts. *Appl. Catal. B* **2007**, *75*, 312–323. [[CrossRef](#)]
50. Sharma, R.; Bansal, S.; Singhal, S. Tailoring the photo-Fenton activity of spinel ferrites (MFe<sub>2</sub>O<sub>4</sub>) by incorporating different cations (M  $\frac{1}{4}$  Cu, Zn, Ni and Co) in the structure. *RSC Adv.* **2015**, *5*, 6006. [[CrossRef](#)]
51. Tamimi, M.; Qourzal, S.; Barka, N.; Assabbane, A.; Ait-Ichou, Y. Methomyl Degradation in Aqueous Solutions by Fenton's Reagent and the Photo-Fenton System. *Sep. Purif. Technol.* **2008**, *61*, 103–108. [[CrossRef](#)]
52. Dutta, B.; Jana, S.; Bhattacharjee, A.; Gütllich, P.; Iijima, S.I.; Koner, S.  $\gamma$ -Fe<sub>2</sub>O<sub>3</sub> nanoparticle in NaY-zeolite matrix: Preparation, characterization and heterogeneous catalytic epoxidation of olefins. *Inorg. Chim. Acta* **2010**, *363*, 696–704. [[CrossRef](#)]
53. Singh, C.; Rubina Chaudhary, R.; Gandhi, K. Preliminary study on optimization of pH, oxidant and catalyst dose for high COD content: Solar parabolic trough collector. *Iran. J. Environ. Health Sci. Eng.* **2013**, *10*, 13–23. [[CrossRef](#)] [[PubMed](#)]
54. Buthiyappan, A.; Abdul Raman, A.; Daud, W.M. Development of an advanced chemical oxidation wastewater treatment system for the batik industry in Malaysia. *RSC Adv.* **2016**, *6*, 25222–25241. [[CrossRef](#)]
55. Bradu, C.; Frunza, L.; Mihalche, N.; Avramescu, S.M.; Neață, M.; Udrea, I. Removal of reactive black 5 azo dye from aqueous solutions by catalytic oxidation using CuO/Al<sub>2</sub>O<sub>3</sub> and NiO/Al<sub>2</sub>O<sub>3</sub>. *Appl. Catal. B* **2010**, *96*, 548–556. [[CrossRef](#)]
56. Pan, W.; Zhang, G.; Zheng, T.; Wang, P. Degradation of p-nitrophenol using CuO/Al<sub>2</sub>O<sub>3</sub> as a Fenton-like catalyst under microwave irradiation. *RSC Adv.* **2015**, *5*, 27043–27051. [[CrossRef](#)]

**Disclaimer/Publisher's Note:** The statements, opinions and data contained in all publications are solely those of the individual author(s) and contributor(s) and not of MDPI and/or the editor(s). MDPI and/or the editor(s) disclaim responsibility for any injury to people or property resulting from any ideas, methods, instructions or products referred to in the content.